

Synthesis and materialization of a reaction-diffusion French flag pattern

Anton Zadorin^{1,2}, Yannick Rondelez^{3,4}, Guillaume Gines³, Vadim Dilhas^{1,2},
 Adrian Zambrano^{1,2}, Jean-Christophe Galas^{1,2,*}, André Estevez-Torres^{1,2,*}

¹Université Pierre et Marie Curie, Laboratoire Jean Perrin, 4 place Jussieu, 75005 Paris, France.

²CNRS, UMR 8237, 75005, Paris, France. ³LIMMS/CNRS-IIS, University of Tokyo,

Komaba 4-6-2 Meguro-ku, Tokyo, Japan. ⁴Ecole supérieure de physique et chimie industrielle, Laboratoire Gulliver, 10 rue Vauquelin, 75005, Paris, France. *To whom correspondence should be addressed; E-mail: jean-christophe.galas@upmc.fr, andre.estevez-torres@upmc.fr.

During embryo development, patterns of protein concentration appear in response to morphogen gradients. The archetypal pattern is the French flag composed of three chemically-distinct zones separated by sharp borders. Chemical concentration serves the underlying cells both as an indicator of location and as a fate selector. This strategy could be advantageously transposed to engineer materials capable of morphogenesis, however synthetic analogues of the French flag, let alone their materialization, have remained elusive. Here we introduce an experimental model of gradient-induced pattern formation and its coupling to a material. We engineered artificial analogues of transcriptional networks based on short DNA single strands that interpret a morphogen gradient. Firstly, bistable networks created immobile, sharp and long-lasting concentration fronts. Secondly, the combination of two bistable circuits generated a French flag pattern whose phenotype was reprogrammed by network mutation. Finally, the patterns controlled the macroscopic organization of a complex material, namely DNA-decorated particles. This experimental framework could be used to test morphogenetic models and design programmable materials capable of morphogenesis.

Biological matter has the astonishing capability of self-constructing into predefined shapes: living embryos develop from a simple form into a complex one through a reproducible process called morphogenesis. The embryo is first structured chemically through pattern formation, a process during which out-of-equilibrium molecular programs generate highly ordered concentration patterns of μm to mm size.¹ In this context, synthesizing concentration patterns using artificial molecular programs^{2–6} has two important goals. First, in a reductionist perspective, it allows testing theoretical models in simplified, yet relevant, experimental conditions.⁷ Second, from a synthetic standpoint,⁸ it enables the conception of a new kind of materials capable of autonomous morphogenesis.

Two archetypal mechanisms account for pattern formation in living systems: the symmetry-breaking Turing mechanism^{9–11} and the processing of positional information.^{12–14} In the latter, a

pre-existing morphogen gradient is interpreted by a molecular program in a reaction-diffusion (RD) process producing several chemically-distinct regions with sharp borders. Lewis Wolpert named this the French Flag problem to illustrate the issue, fundamental because it arises in the development of virtually all complex organisms, of creating three distinct regions of space from an amorphous mass and a shallow concentration gradient (Figure 1A). Well-known examples are provided by the gap gene system in *Drosophila*,¹³ where the three regions become the head, the thorax and the abdomen, and by sonic hedgehog in the patterning of the vertebrate neural tube.¹⁵ Turing patterns were first demonstrated experimentally in a purely chemical system in 1990^{16,17} whereas synthetic systems capable of interpreting a morphogen pre-pattern have remained elusive.

Here we take inspiration from the early development of a living embryo to create a primitive material that self-organizes following two principles acting sequentially: i) pattern formation creates chemically well-defined regions of space and ii) the chemical pattern influences the final structure of an initially homogeneous material. In a learning-by-doing approach to this question^{2-6,18} we set out with the goal of synthesizing a French flag pattern outside of a living organism.

Our design for building a French flag pattern consists of two immobile concentration fronts. The conversion of a shallow morphogen gradient into a concentration boundary that is both sharp and immobile requires a reaction network that interprets the gradient in a non-linear fashion. Diverse evidence¹⁹⁻²¹ suggest that bistability is an essential property of such networks but the role of diffusion during gradient interpretation in living embryos remains controversial.²¹⁻²³ The strong historical influence of the *reaction-only* French flag model, which was initially opposed to the *reaction-diffusion* Turing mechanism,^{9,24} resulted in diffusion being neglected when considering gradient-induced patterning.¹⁹ Modern experiments in *Drosophila* conclude that diffusion is not needed to fit expression data²⁵ but it is necessary to explain the robustness of patterning to fluctuations.¹⁴ In the following, we show experimentally in an artificial system that combining bistability and diffusion yields a robust patterning mechanism, providing evidence for recent hypotheses suggesting that a Turing-Wolpert mechanism could be at play *in vivo*.^{23,24}

DNA oligonucleotides are particularly well suited to construct pattern-forming molecular programs.^{4,18,26,27} On the one hand, the reactivity of the hybridization reaction obeys simple rules and a wide array of methods coming from biotechnology renders their synthesis, analysis and modification straightforward. On the other hand, they can be easily interfaced with materials such as DNA nanostructures,²⁸ aptamers,²⁹ nanoparticles³⁰ and hydrogels.³¹ We thus engineered a series of bistable networks using the PEN DNA toolbox, a molecular programming language designed to construct networks analogous to transcriptional ones but using only simple biochemical reactions³². This technology has recently been applied to construct out-of-equilibrium networks displaying oscillations,^{32,33} bistability³⁴ and traveling concentration waves.^{4,27,35} Figure 1B depicts the simplest bistable network used here, with a first-order positive feedback loop and a non-linear repressor (Extended Data Figures 1-2). The nodes of the network, A_1 and R_1 , are respectively 11 and 15-mer single-stranded DNAs (ssDNAs), analogous to transcription factors. Self-activation is set by T_{A_1} , a 22-mer ssDNA template that plays the role of a gene. Repression is encoded by promoting the degradation of A_1 with a threshold given by R_1 ³⁶ —italized species names indicate concentration throughout the text. Three enzymes —a polymerase, an exonuclease and a nicking enzyme— provide the metabolic functions homologous to the transcription-translation machinery and dissipate free energy from a reservoir of deoxynucleotides (dNTPs). As it happens in transcription networks, A_1 is continuously produced and degraded but the total template —gene— concentration is fixed. In contrast to networks *in vivo*, molecular interactions are well-known and the mechanism and kinetic rates can be precisely deter-

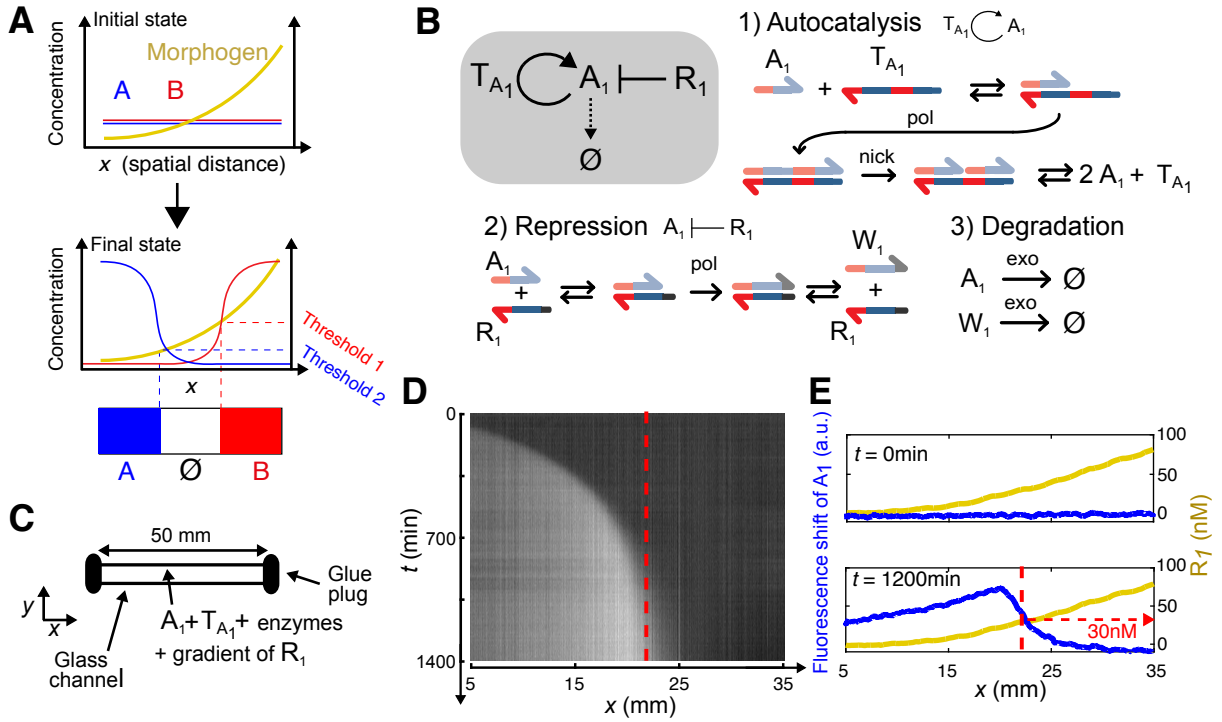


Figure 1: In a shallow gradient of morphogen, a bistable DNA network produces a Polish flag; a sharp and immobile concentration profile. (A) Scheme of Wolpert’s French flag problem, where a gradient of morphogen yields three chemically-distinct zones: blue, white and red. (B) DNA-based bistable network with A_1 self-activation supported by template T_{A_1} , repressed by R_1 and continuously degraded, together with its molecular mechanism. Harpooned thick arrows are ssDNA where colors indicate sequence domains and light hue indicates complementarity. Straight black arrows denote chemical reactions. pol, nick and exo stand for polymerase, nicking enzyme and exonuclease, respectively. W_1 is a waste strand that cannot activate T_{A_1} . (C) Sketch of the experimental setup. (D) Kymograph of the fluorescence shift due to A_1 inside a capillary containing the network in (B) with initial condition $A_1(x, 0) = 1\text{ nM}$ and pre-patterned with the gradient $R_1(x, 0)$ as in (E). The red dashed line indicates the stationary position of the profile. (E) Profiles of R_1 (yellow) and the fluorescence shift due to A_1 (blue) along the channel at initial time and after 1200 min.

mined.³²

Our first goal was to create an immobile concentration front in the presence of a morphogen gradient, which we have called a Polish flag. We performed patterning experiments within 5 cm-long sealed glass microchannels of $4 \times 0.2\text{ mm}^2$ cross-section (Figure 1C). An exponential gradient of morphogen R_1 with a characteristic length $l = 2\text{ cm}$ was generated along the longitudinal axis of the channel by partially mixing two solutions with different R_1 by Taylor dispersion (Figure 1E and Extended Data Figure 3). In this geometry the gradient was stable within 10% over 10 h (Extended Data Figure 3). Initially the channel contained homogeneous concentrations of the three enzymes, dNTPs, $T_{A_1} = 25\text{ nM}$, $A_1 = 1\text{ nM}$, and a gradient of R_1 in the range $0 - 200\text{ nM}$. The evolution of A_1 was measured by adding a fluorescent DNA intercalator and recording time-lapse fluorescence images in an inverted microscope. Figure 1D displays the spatio-temporal dynamics of the patterning process. A short, purely reactional, initial phase generated a sharp profile of A_1 at a location corresponding

to low morphogen concentration (Extended Data Figure 4a). This profile later moved to the right through a reaction-diffusion (RD) mechanism, progressively decelerating until it stopped at the center of the channel at a position where $R_1^{RD} = 30 \pm 5$ nM. The characteristic width of the front was 2 mm, 10-fold sharper than the morphogen gradient, and remained immobile up to 15 h (Extended Data Figure 4b). When, instead of the repressor, the autocatalyst template was used as the morphogen, the complementary Polish flag pattern was obtained (Figure S3-S4). Stationary patterns were observed also when the morphogen gradient was immobilized on a surface (Figure S7).

The gap gene network, which interprets the Bicoid morphogen gradient during the development of the *Drosophila* blastoderm (Figure 2A), is definitely more complex than the bistable network used so far. For instance, Bicoid activates Hunchback, which grows autocatalytically and strongly represses Knirps, which also grows autocatalytically and represses Hunchback.²⁵ We designed a network that mimics these interactions³⁴ (Figures 2B and Extended Data Figure 5) and recorded the patterning dynamics in a gradient of the Bicoid analogue, T_H (Figure 2C-E, Movie S1). At short times, a purely

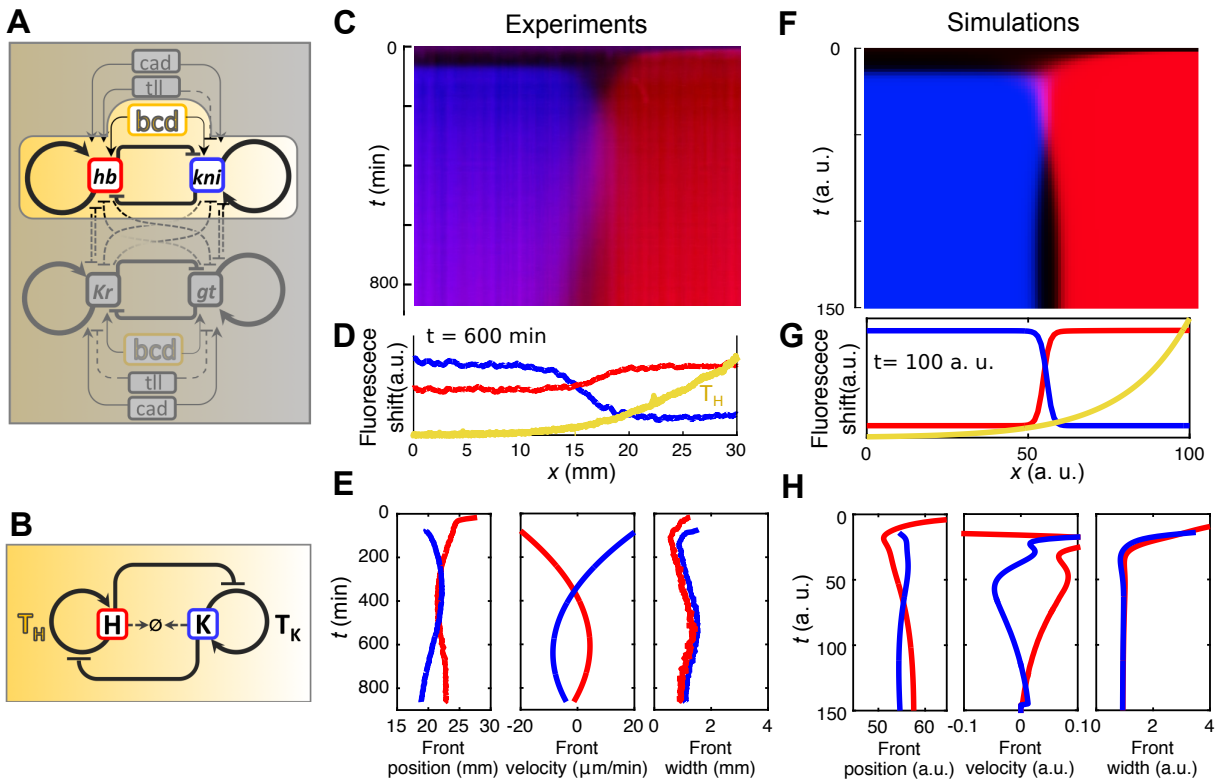


Figure 2: A DNA-based network that mimics part of the gap gene regulatory network generates two fronts that repel each other. (A) Topology of the gap gene network, from²⁵ the portion reproduced here is highlighted. (B) Analogue DNA-based network for the principal interactions between Bicoid, bcd, Hunchback, hb and Knirps, kni. Their DNA counterparts are respectively noted T_H , H and K. Experiments (C, D, E) and simulations (F, G, H) showing the kymograph of the fluorescence shift (C, F) for species H (red) and K (blue) inside a capillary containing the network in (B) and pre-patterned with a gradient of T_H (yellow) and fluorescence shift profiles at $t = 600$ min (D) and $t = 100$ a.u. (G). (E, H) Front position, velocity and width as a function of time extracted from the kymograph (colors as in D and G).

reactional phase created two independent and sharp fronts of the analogues of Hunchback, H, and Knirps, K. Subsequently, during an RD phase, the fronts traveled in opposite directions until they collided in the middle of the channel. At this time, the two profiles partially overlapped and a slow phase made the two fronts go backwards until reaching a steady-state where the overlap disappeared. 1-dimensional simulations with a 4-variable model (see SI Methods) displayed a similar behavior and suggested that this last phase was due to a slow synthesis of the repressors (Figure 2F-H). This patterning process was highly reproducible (Figure S5-S6).

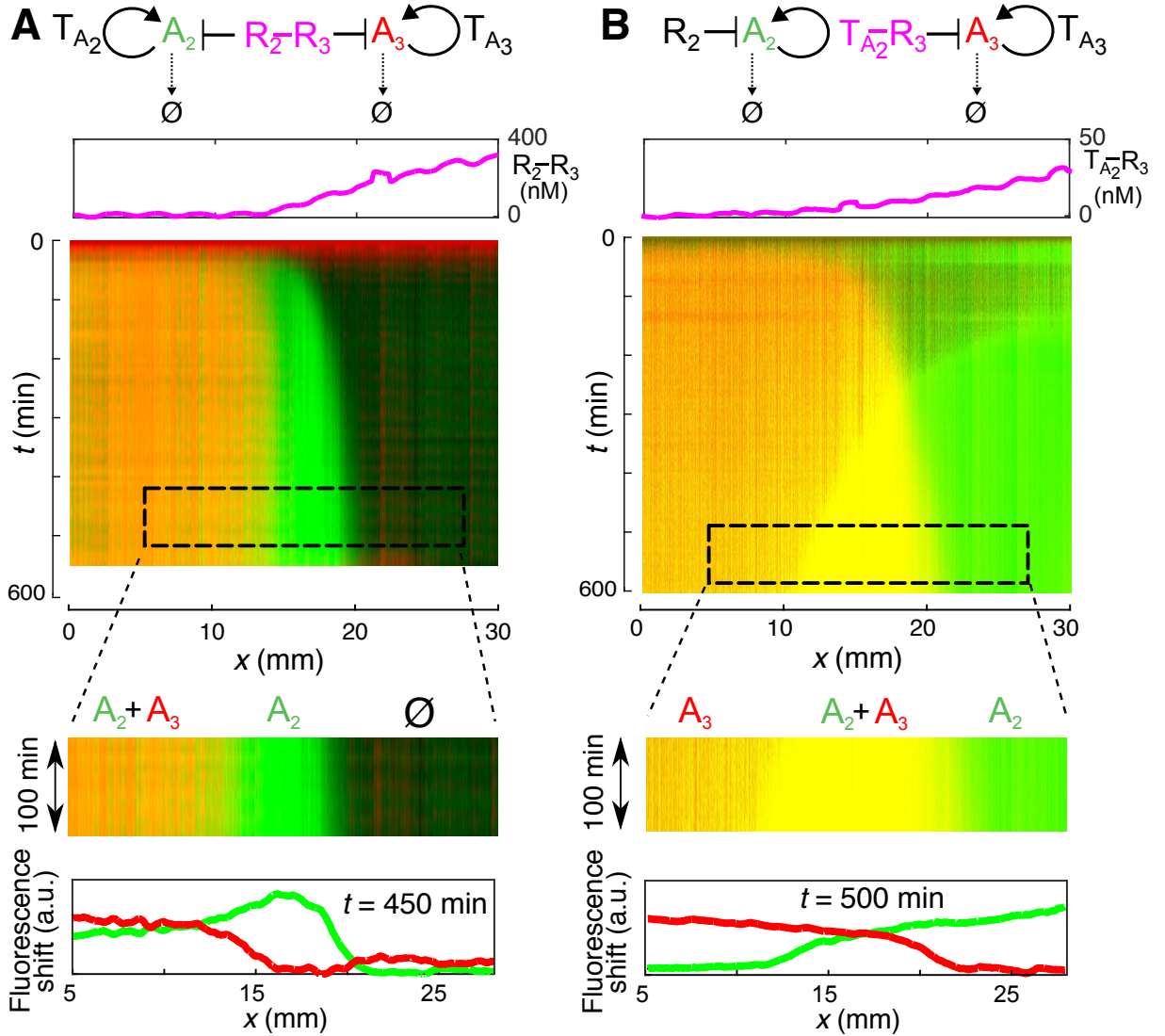


Figure 3: The combination of two orthogonal bistable networks produces a French flag pattern that can be simply reprogrammed. From top to bottom: network topology, initial morphogen gradient, kymograph and fluorescence shift profiles at steady state for two bistables coupled through either a double-repressor strand, $R_2 - R_3$ (**A**), or a template-repressor strand, $T_{A_2} - R_3$ (**B**), each used as morphogen gradient. Dashed rectangles are zooms of the kymographs where the two French flag patterns were stationary.

To implement a French flag pattern with three chemically-distinct zones (Figure 3, Extended Data Figures 6-7 and Movie S2) we combined two orthogonal bistables, A_2 and A_3 , (Figure S8) into a single network using two different approaches. We used a bifunctional morphogen bearing either both repressors, $R_2 - R_3$, or one autocatalyst template and a repressor, $T_{A_2} - R_3$. In a gradient of $R_2 - R_3$, a channel containing a uniform concentration of T_{A_2} and T_{A_3} generated a French flag pattern that divided space into three regions, $A_2 + A_3$, A_2 and \emptyset , for 100 min (Figure 3A). By contrast, with a gradient of $T_{A_2} - R_3$ and a uniform concentration of R_2 and T_{A_3} a different pattern separated the space into A_3 , $A_2 + A_3$ and A_2 .

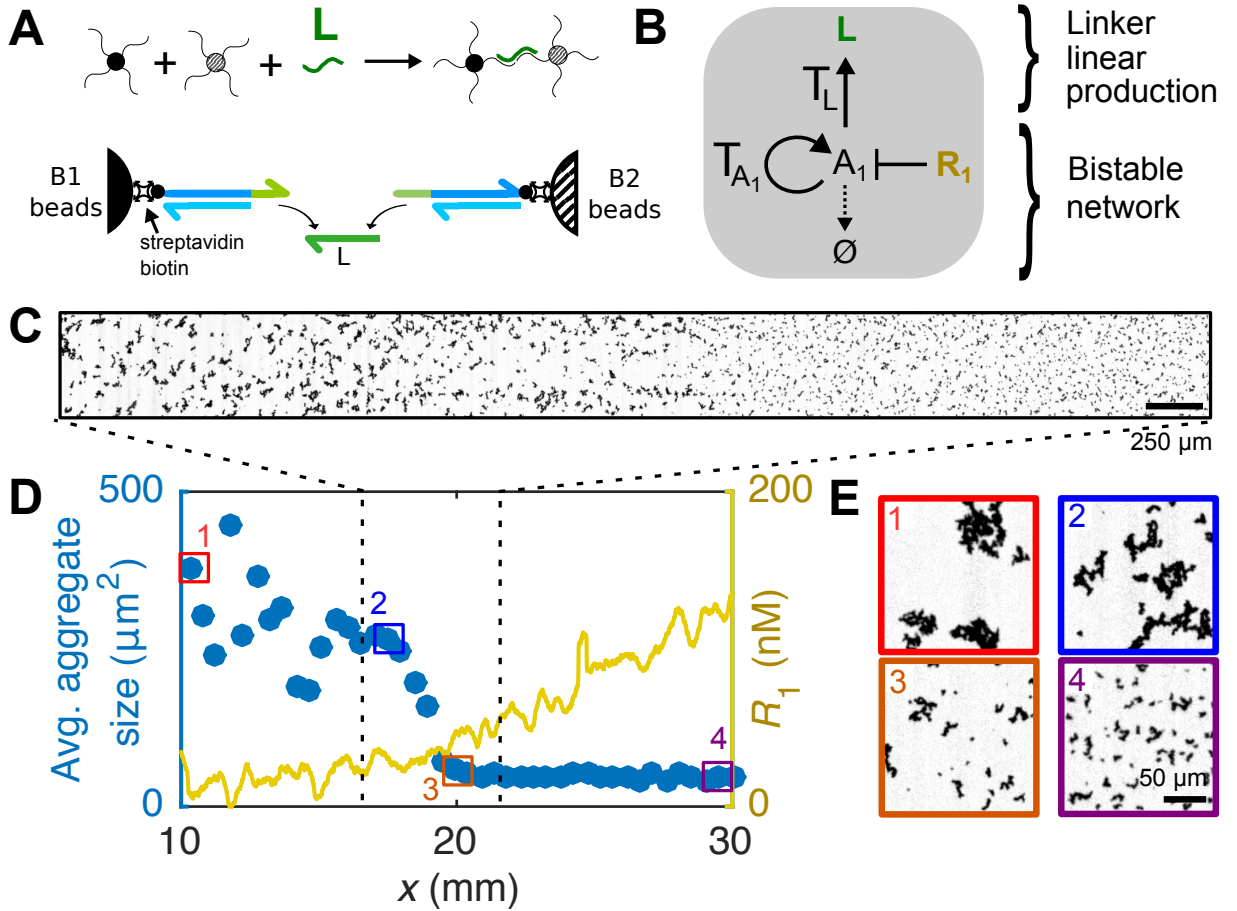


Figure 4: Materialization of a Polish flag pattern with conditional particle aggregation. (A) Sketch of the mechanism of particle aggregation where $1 \mu\text{m}$ particles decorated with two different DNA constructs (black and gray disks) are aggregated in the presence of linker strand L . (B) Scheme of the reaction network used here, where a bistable is coupled to the linear production of L with template T_L . All data were recorded after 40 h from a channel containing the particles, the network in panel (B) and an initial gradient of R_1 . (C) Brightfield image at the center of the channel. (D) Average size of particle aggregates (blue disks, left axis) and initial concentration of R_1 (yellow line, right axis) along the longitudinal axis of the channel. The colored squares indicate the positions at which the brightfield images in (E) were recorded. The dashed lines correspond to the position where (C) was recorded.

In the embryo, pattern formation induces tissue differentiation by providing localized chemical cues to pluripotent cells.¹ Artificial materials inspired by this mechanism would bear astonishing properties, such as the capability to adapt their shape or function to different environmental conditions. As a proof of concept we coupled a Polish flag-generating network to the conditional aggregation of 1 μm diameter beads³⁰ (Figure 4). Streptavidin-labeled particles were decorated with two types of biotin-labeled DNAs that had two different 11-mer ssDNA dangling ends. In the working buffer, the beads aggregated only in the presence of a linker strand L complementary to both ssDNA portions (Extended Data Figure 8). A capillary containing i) a homogeneous dispersion of both types of beads, ii) a bistable network coupled to the linear production of L and iii) a gradient of R₁, produced a Polish flag of bead aggregation (Figure 4C-E). The aggregation pattern was stable for up to a month (Extended Data Figure 9). Interestingly, the width of the aggregation front was 500 μm , 4-fold sharper than the front of fluorescence due to species A₁ in Figure 1. This primitive morphogenetic material thus uses two different sharpening mechanisms. The first one results from coupling the bifurcation of a bistable dynamic system to diffusion while the second is probably due to the cooperativity of bead-bead aggregation. This multi-level sharpening recalls hierarchical patterning mechanisms *in vivo* and could be advantageously used for microfabrication.

Our results demonstrate that DNA-based molecular programming is well suited to engineer concentration patterns reminiscent of those observed during early morphogenesis. They indicate that the combination of a bistable reaction network with diffusion is a simple engineering solution to generate immobile concentration fronts that are both sharp and long lasting. Our experimental model may help understanding the role of regulative and diffusive processes during development and suggests that relatively simple networks may have enabled patterning at an early stage of evolution. Importantly, the simplicity of the method allowed us to record the patterning dynamics in real time, showing that a purely reactional initial phase is followed by a reaction-diffusion one. Finally, by coupling programmable patterns with matter we have engineered a morphogenetic material. This approach could be interfaced with other DNA-compatible materials and devices^{28,29,31} or peptide-based materials³⁷ to create morphogenetic matter.

Acknowledgments

We thank Erwin Frey for insightful discussions, Alexis Vlandas for help with gradient generation and Ben Caller and Damien Woods for comments on the text. Supported by European commission FET-STREP under award Ribonets, by ANR jeunes chercheurs program under award Dynano, and by C'nano Ile-de-France (DNA2PROT grant).

References

- ¹ L. Wolpert and C. Tickle. *Principles of development*. Oxford University Press, Oxford, 2011.
- ² M. Isalan, C. Lemerle, and L. Serrano. Engineering gene networks to emulate drosophila embryonic pattern formation. *PLoS Biol.*, 3(3):488–496, 2005.
- ³ M. Loose, E. Fischer-Friedrich, J. Ries, K. Kruse, and P. Schwille. Spatial regulators for bacterial cell division self-organize into surface waves *in vitro*. *Science*, 320(5877):789–792, 2008.

⁴ A. Padirac, T. Fujii, A. Estevez-Torres, and Y. Rondelez. Spatial waves in synthetic biochemical networks. *J. Am. Chem. Soc.*, 135(39):14586–14592, 2013.

⁵ S. N. Semenov, A. J. Markvoort, T. F. A. de Greef, and W. T. S. Huck. Threshold sensing through a synthetic enzymatic reaction-diffusion network. *Angew. Chem. Int'l. Ed.*, 53(31):8066–8069, 2014.

⁶ A. M. Tayar, E Karzbrun, V. Noireaux, and R. H. Bar-Ziv. Propagating gene expression fronts in a one-dimensional coupled system of artificial cells. *Nat. Phys.*, 11:1037–1041, 2015.

⁷ Nathan Tompkins, Ning Li, Camille Girabawe, Michael Heymann, G. Bard Ermentrout, Irving R. Epstein, and Seth Fraden. Testing Turing's theory of morphogenesis in chemical cells. *Proceedings of the National Academy of Sciences*, 10.1073/pnas.1322005111, 2014.

⁸ Ryo Yoshida, Toshikazu Takahashi, Tomohiko Yamaguchi, and Hisao Ichijo. Self-oscillating gel. *Journal of the American Chemical Society*, 118(21):5134–5135, 1996.

⁹ A. M. Turing. The chemical basis of morphogenesis. *Phil. Trans. Roy. Soc. B*, 237(641):37–72, 1952.

¹⁰ R. Sheth, L. Marcon, M. F. Bastida, M. Junco, L. Quintana, R. Dahn, M. Kmita, J. Sharpe, and M. A. Ros. Hox genes regulate digit patterning by controlling the wavelength of a Turing-type mechanism. *Science*, 338(6113):1476–1480, 2012.

¹¹ A. D. Economou, A. Ohazama, T. Porntaveetus, P. T. Sharpe, S. Kondo, M. A. Basson, A. Gritli-Linde, M. T. Cobourne, and J. B. A. Green. Periodic stripe formation by a Turing mechanism operating at growth zones in the mammalian palate. *Nature Genetics*, 44(3):348–351, 2012.

¹² L. Wolpert. Positional information and the spatial pattern of cellular differentiation. *J. Theo. Biol.*, 25(1):1–47, 1969.

¹³ D. St Johnston and C. Nüsslein-Volhard. The origin of pattern and polarity in the drosophila embryo. *Cell*, 68(2):201–219, 1992.

¹⁴ T. Gregor, D. W. Tank, E. F. Wieschaus, and W. Bialek. Probing the limits to positional information. *Cell*, 130(1):153–64, 2007.

¹⁵ E. Dessaoud, A. P. McMahon, and J. Briscoe. Pattern formation in the vertebrate neural tube: a sonic hedgehog morphogen-regulated transcriptional network. *Development*, 135(15):2489–503, 2008.

¹⁶ V. Castets, E. Dulos, J. Boissonade, and P. De Kepper. Experimental evidence of a sustained standing Turing-type nonequilibrium chemical pattern. *Phys. Rev. Lett.*, 64(24):2953, 1990.

¹⁷ Q. Ouyang and H. L. Swinney. Transition from a uniform state to hexagonal and striped Turing patterns. *Nature*, 352(6336):610–612, 1991.

¹⁸ S. M. Chirieleison, P. B. Allen, Z. B. Simpson, A. D. Ellington, and Xi C. Pattern transformation with DNA circuits. *Nat Chem*, 5(12):1000–1005, 2013.

¹⁹ P. Fran cois, V. Hakim, and E. D. Siggia. Deriving structure from evolution: metazoan segmentation. *Mol Syst Biol*, 3:154, 2007.

²⁰ F. J. Lopes, F. M. Vieira, D. M. Holloway, P. M. Bisch, and A. V. Spirov. Spatial bistability generates hunchback expression sharpness in the drosophila embryo. *PLoS Comput Biol*, 4(9):e1000184, 2008.

²¹ S. Rulands, B. Klünder, and E. Frey. Stability of localized wave fronts in bistable systems. *Phys. Rev. Lett.*, 110(3):038102, 2013.

²² J. Jaeger, Manu, and J. Reinitz. Drosophila blastoderm patterning. *Curr. Opin. Genet. Dev.*, 22(6):533–41, 2012.

²³ C. Quiñinao, A. Prochiantz, and J. Touboul. Local homeoprotein diffusion can stabilize boundaries generated by graded positional cues. *Development*, 142(10):1860–8, 2015.

²⁴ J. B. Green and J. Sharpe. Positional information and reaction-diffusion: two big ideas in developmental biology combine. *Development*, 142(7):1203–11, 2015.

²⁵ Manu, S. Surkova, A. V. Spirov, V. V. Gursky, H. Janssens, A. Kim, O. Radulescu, C. E. Vanario-Alonso, D. H. Sharp, M Samsonova, and J. Reinitz. Canalization of gene expression and domain shifts in the drosophila blastoderm by dynamical attractors. *PLoS Comput Biol*, 5(3):e1000303, 2009.

²⁶ Dominic Scalise and Rebecca Schulman. Designing modular reaction-diffusion programs for complex pattern formation. *Technology*, 02(01):55–66, 2014.

²⁷ A. S. Zadorin, Y. Rondelez, J.-C. Galas, and A. Estevez-Torres. Synthesis of programmable reaction-diffusion fronts using DNA catalysts. *Phys. Rev. Lett.*, 114(6):068301, 2015.

²⁸ P. W. K. Rothenmund. Folding DNA to create nanoscale shapes and patterns. *Nature*, 440(7082):297–302, 2006.

²⁹ E. Franco, E. Friedrichs, J. Kim, R. Jungmann, R. Murray, E. Winfree, and F. C. Simmel. Timing molecular motion and production with a synthetic transcriptional clock. *Proc. Natl. Acad. Sci. USA*, 10.1073/pnas.1100060108, 2011.

³⁰ C. A. Mirkin, R. L. Letsinger, R. C. Mucic, and J. J. Storhoff. A DNA-based method for rationally assembling nanoparticles into macroscopic materials. *Nature*, 382(6592):607–609, 1996.

³¹ J. B. Lee, S. Peng, D. Yang, Young H. Roh, H. Funabashi, N. Park, E. J. Rice, L. Chen, R. Long, M. Wu, and D. Luo. A mechanical metamaterial made from a DNA hydrogel. *Nat. Nano*, 7(12):816–820, 2012.

³² K. Montagne, R. Plasson, Y. Sakai, T. Fujii, and Y. Rondelez. Programming an in vitro DNA oscillator using a molecular networking strategy. *Mol Syst Biol*, 7:466, 2011.

³³ T. Fujii and Y. Rondelez. Predator-prey molecular ecosystems. *ACS Nano*, 7(1):27–34, 2013.

³⁴ A. Padirac, T. Fujii, and Y. Rondelez. Bottom-up construction of in vitro switchable memories. *Proc. Natl. Acad. Sci. USA*, 10.1073/pnas.1212069109, 2012.

³⁵ A. Zambrano, A. S. Zadorin, Y. Rondelez, A. Estevez-Torres, and J. C. Galas. Pursuit-and-evasion reaction-diffusion waves in microreactors with tailored geometry. *J. Phys. Chem. B*, 119(17):5349–5355, 2015.

³⁶ Kevin Montagne, Guillaume Gines, Teruo Fujii, and Yannick Rondelez. Boosting functionality of synthetic dna circuits with tailored deactivation. *Nature Communications*, 7:13474, 2016.

³⁷ K. E. Inostroza-Brito, E. Collin, O. Siton-Mendelson, K. H. Smith, A. Monge-Marcet, D. S. Ferreira, R. P. Rodriguez, M. Alonso, J. C. Rodriguez-Cabello, R. L. Reis, F. Sagues, L. Botto, R. Bitton, H. S. Azevedo, and A. Mata. Co-assembly, spatiotemporal control and morphogenesis of a hybrid protein-peptide system. *Nat Chem*, 7(11):897–904, 2015.

Methods

DNA strands were purchased from Biomers (Ulm, Germany). The Bst DNA polymerase and the two nicking enzymes (Nb.BsmI and Nt.BstNBI) were purchased from New England Biolabs. The *Thermus thermophilus* RecJ exonuclease was expressed in *E. coli* and purified by chromatography according to a published protocol.⁷ Experiments were performed at 45 °C for the Polish and French flag generating networks and at 42 °C for the gap gene-like network. Details on the the sample preparation, the DNA sequences, the experimental conditions, the data analysis and the simulations are provided in the Supplementary Information.

Particle suspension. 1 μ m diameter, streptavidin-coated, paramagnetic beads (Dynabeads MyOne C1, Invitrogen) were functionalized with two types of biotinylated DNA constructs, as described,⁷ making two types of beads, B1 and B2. Each construct consists of a 49 bp-long dsDNA backbone terminated with an 12 bases-long single stranded sticky end. The construct corresponding to B1 (resp. B2) was biotin-labeled on the 5' end (resp. 3' end) and the corresponding sticky end was on the 3' side (resp. 5' side). Such a design implies that the DNA-decorated beads will be stable in solution when mixed, unless the linker strand complementary to the sticky ends of each bead type is present.

Measurement of DNA concentrations. DNA concentrations were measured by fluorescence. We used three different strategies. i) Recording the green fluorescence, proportional to the concentration of double stranded DNA, from EvaGreen dye (Biotium). ii) Recording the fluorescence from dyes attached to the 3' or 5' end of template strands (see Table S2 for details). When the corresponding inputs or outputs hybridize on these templates fluorescence is quenched. iii) The concentrations of morphogen were measured by adding 1 μ M of cascade blue-dextran $M_w = 3000$ Da (Thermo Fisher Scientific) to the solution with high concentration of morphogen used to generate the gradient, and recording its fluorescence in real time. The cascade blue-dextran has a molecular weight similar to the DNA templates and thus a similar diffusion coefficient, as verified in a control experiment. In all kymographs and plots we represented the absolute value of the fluorescence shift, which is proportional to the concentration of fluorescent species for both cases.

Generation of the morphogen gradient. Spatiotemporal (1D) experiments were performed within 50 mm \times 4 mm \times 0.2 mm glass capillaries (Vitrocom USA). The capillary was loaded using a micropipette and a custom-made PDMS connector. The capillary was filled with 45 μ L of the reaction solution without morphogen strand and then a pipette was inserted being in the 'push' position into the PDMS connector. The other end of the capillary was dipped into the reaction solution containing the morphogen DNA strand. 15 up-and-down pumps of 12.5 μ L of solution were performed to create the gradient. Finally, the pipette was left in the 'pulled' position and the pipette together with the PDMS connector were removed. Extended Data Figure 3a shows two methylene blue dye gradients prepared this way.

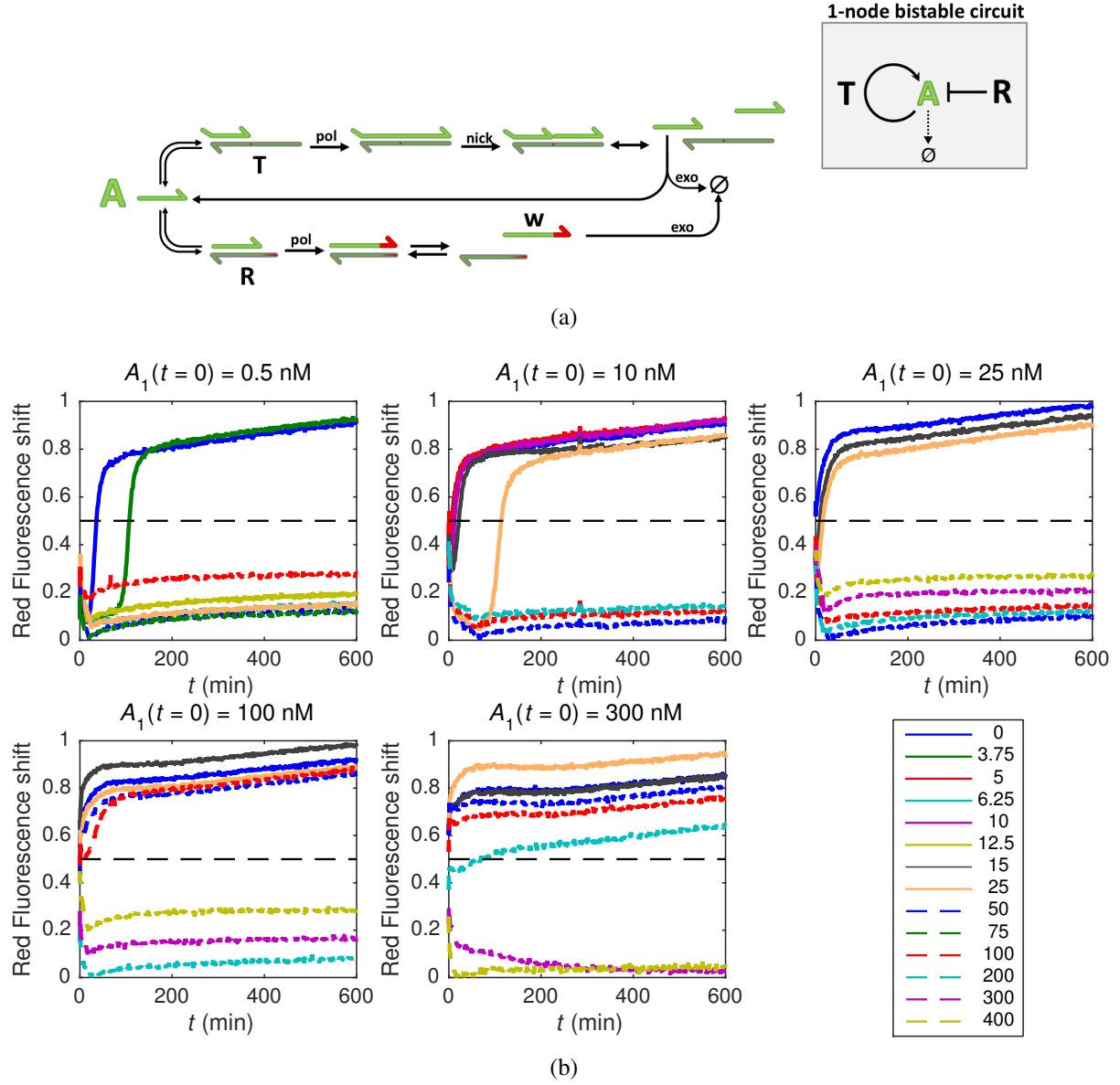
Microscopy. Once the gradient was formed, the capillary was laid on a 5 \times 7.5 cm glass slide. 5-minutes Araldite epoxy was used both to seal the capillary ends and to glue them to the glass slide. No evaporation at all was observed for 48 h at 45°C. The fluorescence along the capillary was recorded on a Zeiss Axio Observer Z1 fully automated epifluorescence microscope equipped with a CoolLED pE-2 fiber-coupled illuminator, DAPI, GFP, YFP and RFP filter sets, a Marzhauser XY motorized stage,

a Tokai Hit thermo plate, and Andor iXon Ultra 897 EMCCD camera, a shutter and a $2.5\times$ objective. These instruments were controlled with MicroManager 1.4. For optimal thermal conduction, mineral oil was added between the glass slide and the thermoplate on the microscope, and also between the glass slide and the capillary. For each capillary, 16 contiguous $3.17\times3.17\text{ mm}^2$ ($128\times128\text{ pixel}^2$) images were recorded automatically every 1 to 10 minutes. Multi-color fluorescence microscopy was used to record the concentration of different DNA species over time. Images of the beads were acquired in bright field with a 10 or a $40\times$ objective.

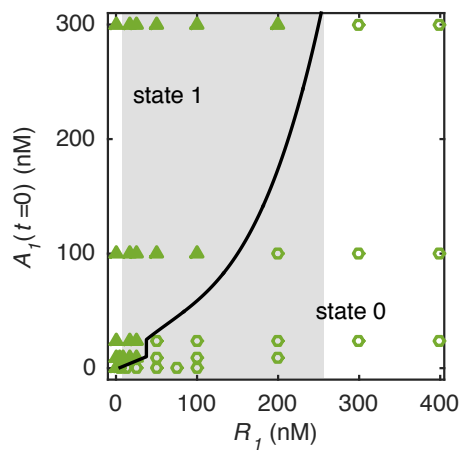
Image treatment. The raw data were treated with ImageJ / Fiji (NIH) and Matlab (The Mathworks). Prior to data analysis, the 16 images making one capillary were stitched together without overlapping. Subsequently, the inhomogeneous illumination was corrected by two different protocols. When the initial concentration was flat (for all species except for the morphogen) a division by the first frame was performed. When the initial concentration was not homogeneous, for example for the morphogen, a polynome was fitted to the raw data of one of the $3.17\times3.17\text{ mm}^2$ of the first frame and each image was divided by it.

Data treatment. Considering the $50\text{ mm}\times4\text{ mm}$ capillary as a 1D reactor, we first averaged the corrected fluorescence images over the width of the capillary (along the y axis). The kymographs were obtained by stacking these profiles over time. To obtain the front position and width, the profiles averaged along y were further averaged along the x axis by performing a moving average over 25 pixels and subsequently normalized between 0 and 1. A sigmoid function $f(x) = \frac{1}{1+e^{b*(-x+x_0)}}$ was fitted to these data. The front position corresponds to x_0 while the width of the front is defined as $1/b$. To determine the front velocity, the data of front position over time were fitted by a polynomial function to reduce noise. The velocity was calculated as the time derivative of this polynomial fit.

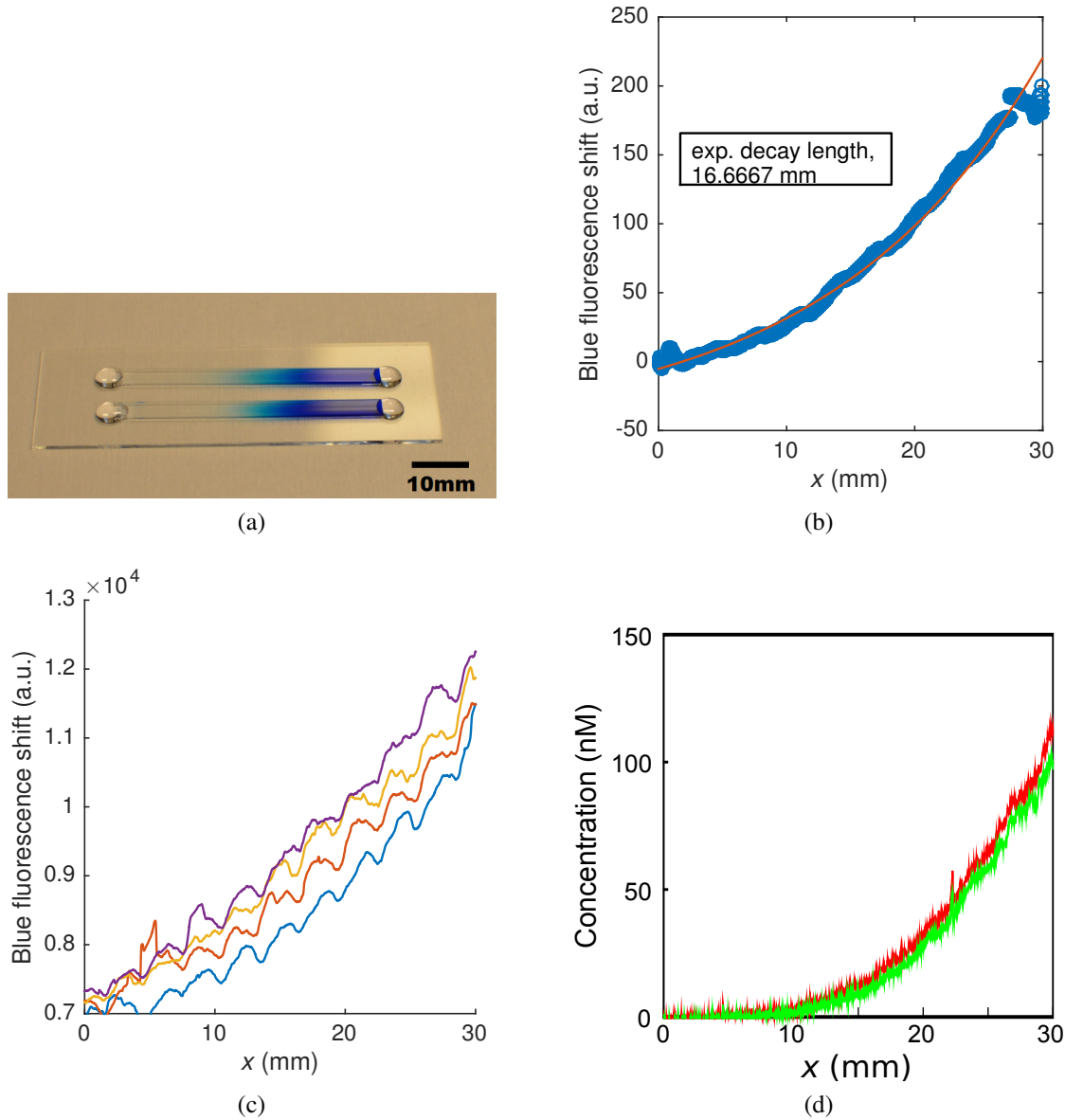
Extended data



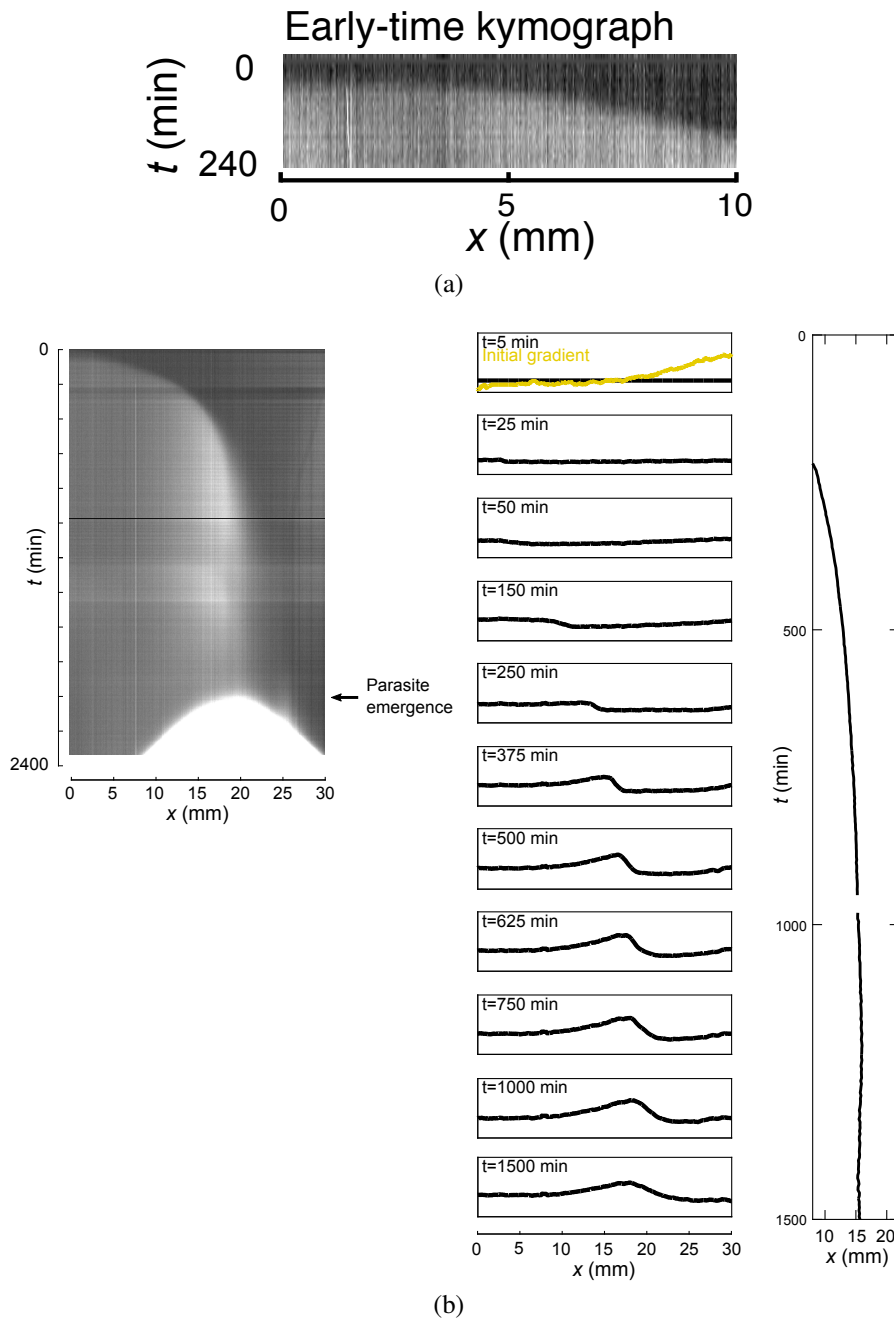
Extended Data Figure 1: Detailed mechanism (a) and 0-dimensional dynamics (b) of the 1-species bistable circuit. (a) The inset reminds the topology of the network. This circuit uses a single auto-catalytic template T producing A exponentially, coupled to a species-specific degradation mechanism driven by the repressor R. Only species that are not protected on the 5' end are degraded by the exonuclease (the top strands). This molecular program admits 2 stable states, defined by the amplification and non-amplification of the A strand. (b) Dynamics of the 1-species bistable for different initial conditions and different thresholded degradation rates. Red fluorescence shift coming from Cy35 dye *vs* time. Each plot represents a different initial condition of A_1 as indicated in the title and each curve represents a different thresholded degradation rate given by the concentration of species R_1 (see legend, in nM). When the final fluorescence shift was above the dashed black horizontal line the bistable was considered to be in state 1 (high) and otherwise in state 0 (low). $T = 45^\circ$, $T_{A_1} = 25$ nM.



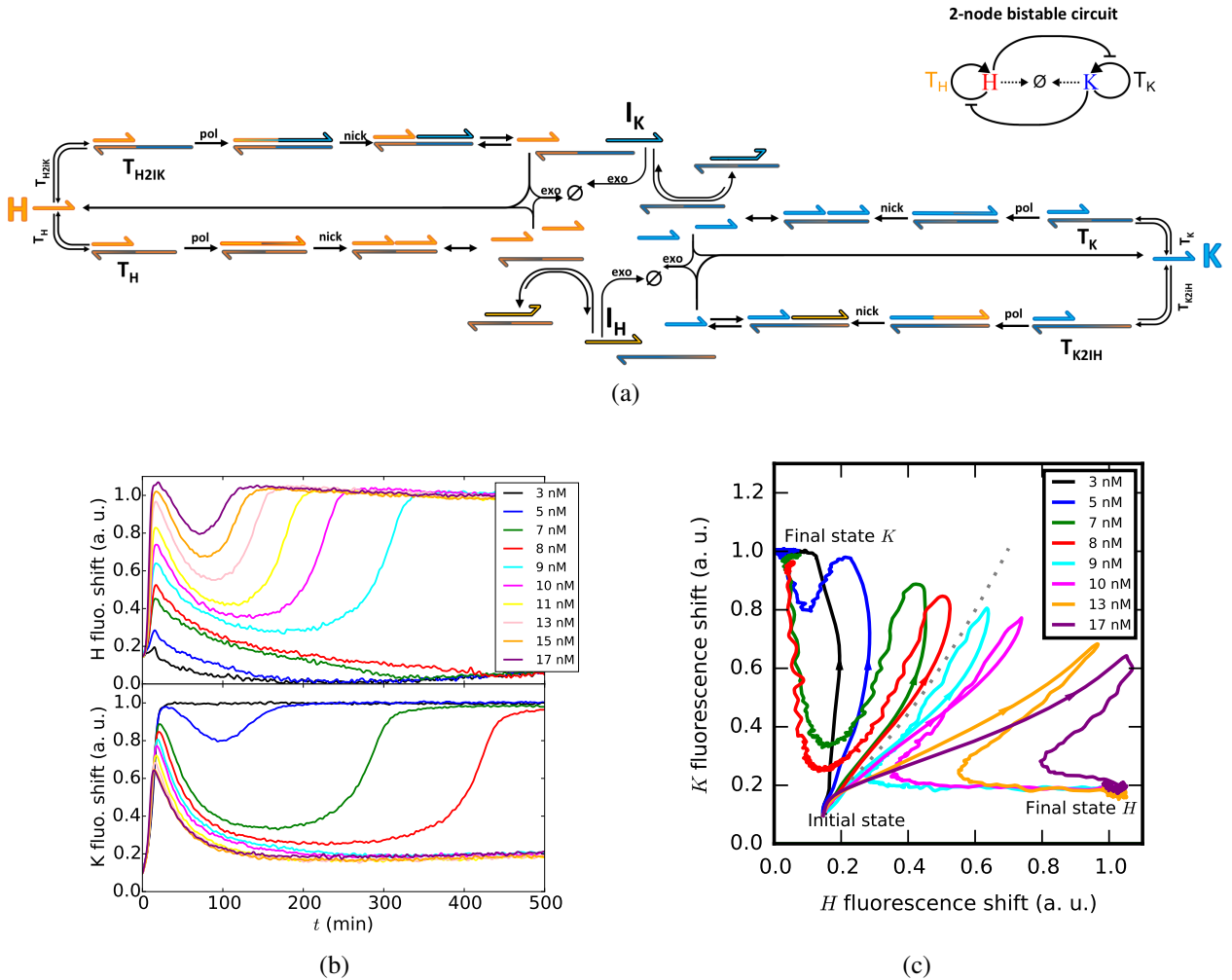
Extended Data Figure 2: Phase space of the 1-species bistable network as a function of repressor concentration, R_1 , and initial condition $A_1(t = 0)$. Triangles and circles correspond to systems ending in the high and low concentration state, respectively. The shaded region indicates the range of R_1 where the system is bistable. Plotted from data in Extended Data Figure 1.



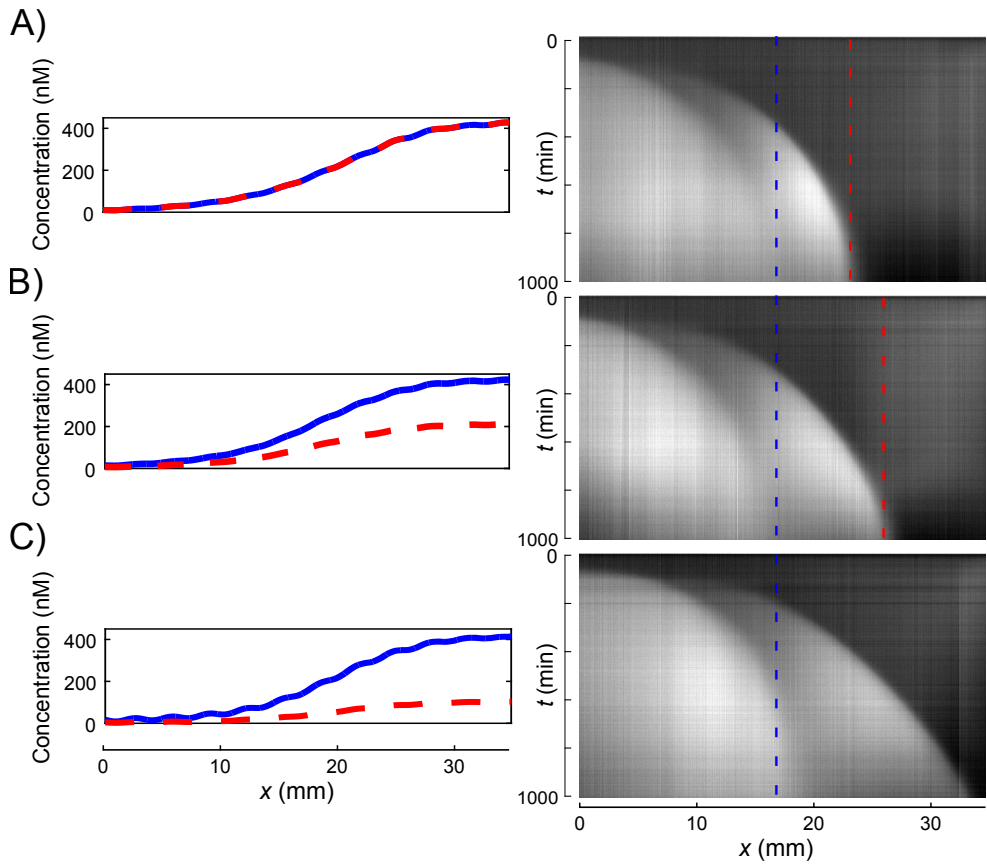
Extended Data Figure 3: Characterization of the morphogen gradient. (a) Gradients of methylene blue dye generated inside the glass capillaries by pipetting back and forth a constant volume of dye. Each extremity of the capillary is sealed with a droplet of glue that serves also to attach it to a glass slide. Methylene blue is not present in the experiments and is used here solely for visualization. (b) The characteristic length of the morphogen gradient is 17 mm. Exponential fit (red line) to the fluorescence intensity from the cascade-blue-dextran gradient in Figure 1 of the Main Text. (c) The generation of the morphogen gradient is fairly reproducible. Fluorescence profiles of cascade-blue-dextran gradients in four different channels prepared at the same time. The gradients were slide-averaged over 25 pixels. The sawtooth shape of the curves is due to illumination inhomogeneities that were not corrected here. (d) The morphogen gradient in solution is stable over the duration of the experiment. Concentration profile within the channel of a 22-mer fluorescently-labeled oligonucleotide at $t = 30$ min (green) and $t = 10$ h (red). $T = 42^\circ\text{C}$.



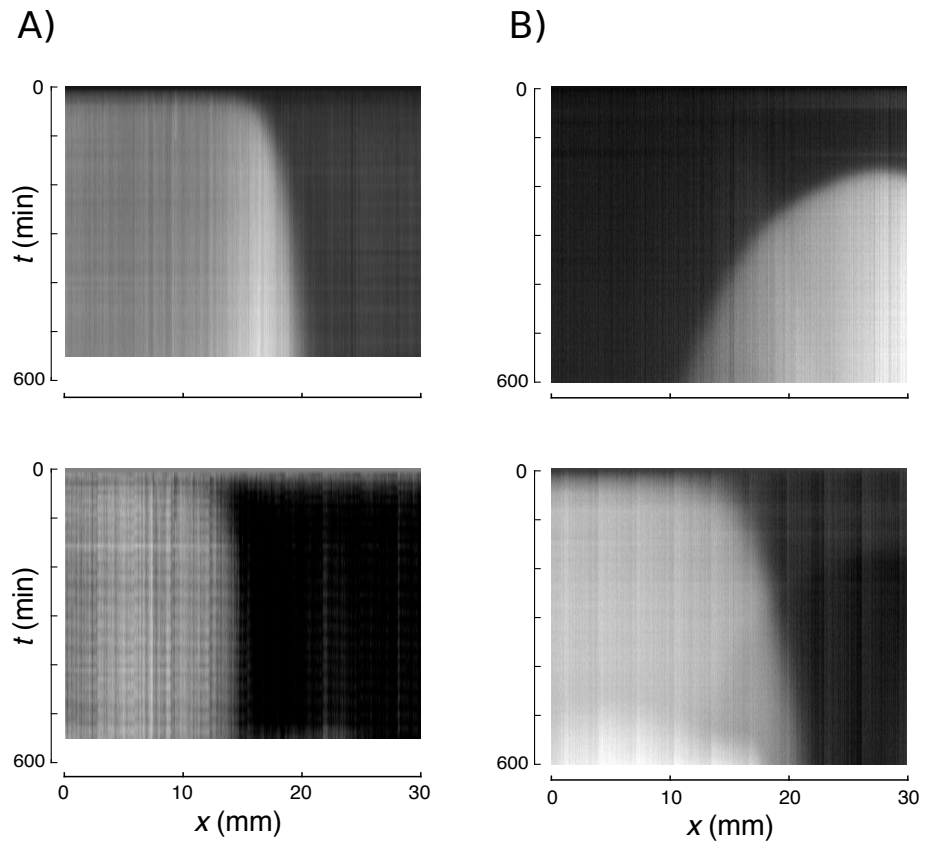
Extended Data Figure 4: Short time and long time behavior of the Polish flag pattern. (a) Kymograph of Figure 1 at short times. At $t \approx 70$ min a purely reaction mechanism creates a front at $x \approx 5$ mm. Later this front moves slowly through a reaction-diffusion mechanism from left to right. (b) Polish flag patterning lasts up to 30 h. Experiment similar to the one shown in Figure 1D-E in the Main Text. Each panel represents the kymograph (left), the fluorescence profiles along the channel at different times (center) with EvaGreen fluorescence in black and morphogen fluorescence in yellow (this last one only at initial time), and the position of the front (right). The fluorescence of EvaGreen is proportional to the concentration of dsDNA in the capillary. At 2000 min a strongly fluorescent species, called a 'parasite', emerges and kills the immobile front, see Supplementary Materials for a discussion. Network Ib with $R_2 = 0 - 400$ nM, and initial constant concentrations of $T_{A_1} = 25$ nM and $A_1 = 0.5$ nM. $T = 45^\circ\text{C}$.



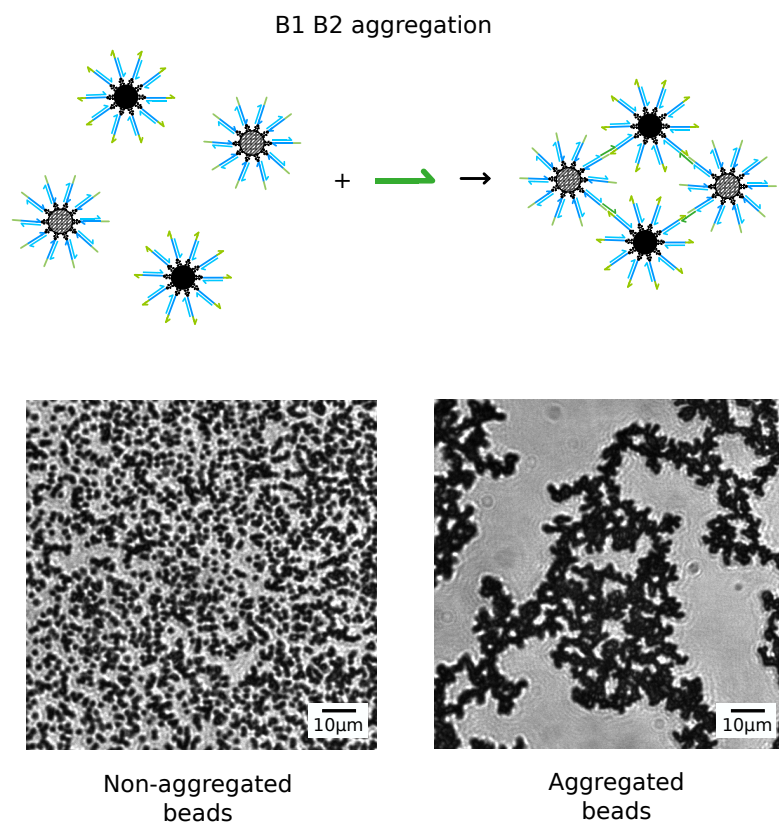
Extended Data Figure 5: Detailed mechanism (a) and 0-dimensional dynamics (b, c) of the 2-species bistable circuit. (a) The inset reminds the simplified topology. This circuit uses 4 catalytic templates: T_H and T_K catalyze the exponential amplification of H and K respectively. The templates T_{H2IK} and T_{K2IH} initiate the synthesis of I_K and I_H , using respectively H and K strands as input. I_K and I_H are able to bind the cognate autocatalytic template with a higher affinity than their input, preventing therefore the amplification of the H and K nodes. Only species that are not protected on the 5' end are degraded by the exonuclease (the top strands). By mixing these 4 templates, a 2-species bistable circuit is obtained, leading to 2 stable states where either H or K are amplified, depending on the experimental initial conditions. (b) The concentration of T_H is a bifurcation parameter for the network in panel a. Fluorescence shift due to species H (top) and K (bottom) as a function of time in well-mixed conditions. Curves with same colors refer to identical experiments, each with a different concentration of template T_H that controls the growth rate of H. When the concentration of T_H is 8 nM or less, K grows and H dies and the final state is $(H, K) = (0, 1)$. When the concentration of T_H is 9 nM or more, K dies and H grows and the final state is $(H, K) = (1, 0)$. $T = 42^\circ$, $T_K = 20$ nM, $T_{H2R_K} = 20$ nM, $T_{K2R_H} = 20$ nM, initial conditions $H = K = 0.5$ nM. (c) Phase portrait from data in panel b. The dashed line separates the T_H values for which the final state is K and those for which the final state is H.



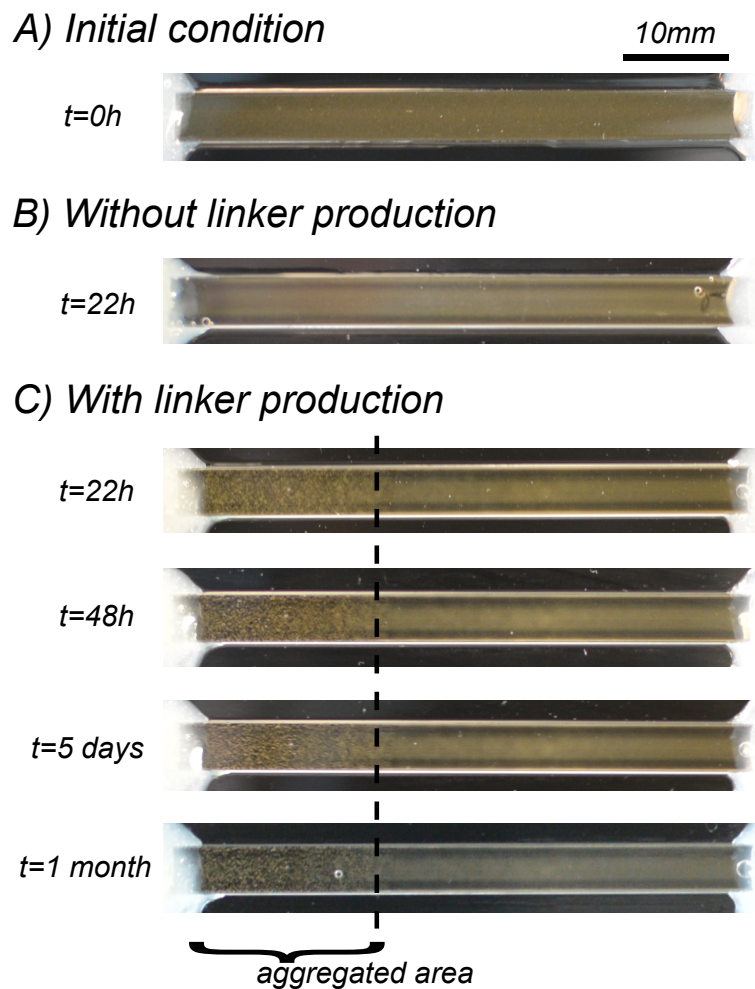
Extended Data Figure 6: Two orthogonal 1-species bistable networks produce a two fronts pattern which position can be independently controlled. Networks Ib and VI (Figure S2) were introduced in a capillary. Two morphogens were used, R_2 and R_3 and gradients of similar shape but different maximal concentrations were generated. The concentration of dsDNA was followed by measuring EvaGreen fluorescence. As the two 1-species bistable networks are orthogonal, changing the morphogen gradient of one of the two networks only affects the position of the corresponding front, that moves to the right. Initial morphogen gradients (left) and Eva Green fluorescence kymographs showing simultaneously the emergence of the two immobile fronts (right) for three different maximum values of repressor R_2 (red dashed lines): 400 (A), 200 (B) and 100 nM (C). In (C) the level of R_2 is too low to stop the front. $T_{A_2} = T_{A_3} = 25$ nM, $A_2 = A_3 = 0.5$ nM, $R_3 = 0 - 400$ nM (blue lines). $T = 45^\circ\text{C}$.



Extended Data Figure 7: Two French flag patterns are presented in Figure 3 of the Main Text. They come from the combination of two orthogonal 1-species bistable networks, one containing species A_2 and the other species A_3 . To follow independently the concentration of A_2 and A_3 the T_{A_3} was labeled with a yellow DY530 dye in 5'. T_{A_2} was not labeled. It appeared that in presence of EvaGreen, only the A_2 system fluoresced in green, while only the A_3 fluoresced in yellow. Here we show separately the two fluorescence channels that were recorded independently during each experiment and that correspond to each bistable for the French flag patterns in Figure 3 of the Main Text. Kymographs for each color channels for the three French Flag patterns. Top row: green fluorescence, corresponding to species A_2 . Bottom row: yellow fluorescence, corresponding to species A_3 .



Extended Data Figure 8: Brightfield microscopy images show non-aggregated and aggregated beads after 1000 min incubation respectively in the absence (left) and in the presence of 1 μ M L (right) in the 1-species bistable buffer without enzymes at 45°C.



Extended Data Figure 9: The morphogenetic aggregation of beads is irreversible and visible to the naked eye. A) At $t = 0$, the dispersion of beads in the capillaries appears as a brown homogeneous background. B) After 22 h, in the presence of 1-species bistable network that does not produce linker L, the beads sediment homogeneously along the longitudinal axis of the capillary but away from the walls and do not aggregate. C) In contrast, in the presence of the 1-species bistable network that does produce linker L, the bead aggregation is clearly seen on the left hand side of the capillary. The pattern of bead aggregation is stable for at least one month. The photos were taken in brightfield with a Nikon D600 camera equipped with a 35 mm lens.